Redox Biology 60 (2023) 102604

Contents lists available at ScienceDirect

Redox Biology

journal homepage: www.elsevier.com/locate/redox

Chemogenetic emulation of intraneuronal oxidative stress affects synaptic plasticity

Andrei L. Kalinichenko [a,b,1], David Jappy [c,d,1], Georgy M. Solius [a,1], Dmitry I. Maltsev [a,c], Yulia A. Bogdanova [a,e], Liana F. Mukhametshina [a,b], Rostislav A. Sokolov [e,f], Aleksandr A. Moshchenko [c], Vladimir A. Shaydurov [c,g], Andrei V. Rozov [c,h,***], Oleg V. Podgorny [a,c,i,*], Vsevolod V. Belousov [a,c,i,j,**]

[a] Shemyakin-Ovchinnikov Institute of Bioorganic Chemistry, Russian Academy of Sciences, 117997, Moscow, Russia
[b] Lomonosov Moscow State University, 119991, Moscow, Russia
[c] Institute of Fundamental Neurology, Federal Center of Brain Research and Neurotechnologies, Federal Medical Biological Agency, 117997, Moscow, Russia
[d] Kazan Federal University, 420008, Kazan, Russia
[e] Pirogov Russian National Research Medical University, 117997, Moscow, Russia
[f] Institute of Biology and Biomedicine, Lobachevsky State University of Nizhny Novgorod, 603022, Nizhny Novgorod, Russia
[g] Institute of Higher Nervous Activity and Neurophysiology, Russian Academy of Sciences, 117485, Moscow, Russia
[h] Institute for Physiology and Pathophysiology, University of Heidelberg, 69120, Heidelberg, Germany
[i] Center for Precision Genome Editing and Genetic Technologies for Biomedicine, Pirogov Russian National Research Medical University, 117997, Moscow, Russia
[j] Institute for Cardiovascular Physiology, Georg August University Göttingen, D-37075, Göttingen, Germany

ARTICLE INFO

Keywords:
Oxidative stress
Synaptic plasticity
Brain aging
Neurodegeneration
Long-term potentiation
Hydrogen peroxide
D-amino acid oxidase

ABSTRACT

Oxidative stress, a state of disrupted redox signaling, reactive oxygen species (ROS) overproduction, and oxidative cell damage, accompanies numerous brain pathologies, including aging-related dementia and Alzheimer's disease, the most common neurodegenerative disorder of the elderly population. However, a causative role of neuronal oxidative stress in the development of aging-related cognitive decline and neurodegeneration remains elusive because of the lack of approaches for modeling isolated oxidative injury in the brain. Here, we present a chemogenetic approach based on the yeast flavoprotein D-amino acid oxidase (DAAO) for the generation of intraneuronal hydrogen peroxide (H_2O_2). To validate this chemogenetic tool, DAAO and HyPer7, an ultrasensitive genetically encoded H_2O_2 biosensor, were targeted to neurons. Changes in the fluorescence of HyPer7 upon treatment of neurons expressing DAAO with D-norvaline (D-Nva), a DAAO substrate, confirmed chemogenetically induced production of intraneuornal H_2O_2. Then, using the verified chemogenetic tool, we emulated isolated intraneuronal oxidative stress in acute brain slices and, using electrophysiological recordings, revealed that it does not alter basal synaptic transmission and the probability of neurotransmitter release from presynaptic terminals but reduces long-term potentiation (LTP). Moreover, treating neurons expressing DAAO with D-Nva via the patch pipette also decreases LTP. This observation indicates that isolated oxidative stress affects synaptic plasticity at single cell level. Our results broaden the toolset for studying normal redox regulation in the brain and elucidating the role of oxidative stress to the pathogenesis of cognitive aging and the early stages of aging-related neurodegenerative diseases. The proposed approach is useful for identification of early markers of neuronal oxidative stress and may be used in screens of potential antioxidants effective against neuronal oxidative injury.

Abbreviations: ACSF, artificial cerebrospinal fluid; AAV, adeno-associated virus; DAAO, D-amino acid oxidase; D-Ala, D-alanine; D-Nva, D-norvaline; D-Ser, D-serine; EPSCs, excitatory postsynaptic currents; H_2O_2, hydrogen peroxide; LTP, long-term potentiation; RFP, red fluorescent protein; ROI, region of interest; ROS, reactive oxygen species.

* Corresponding author. Shemyakin-Ovchinnikov Institute of Bioorganic Chemistry, Russian Academy of Sciences, 117997, Moscow, Russia.
** Corresponding author. Institute of Fundamental Neurology, Federal Center of Brain Research and Neurotechnologies, Federal Medical Biological Agency, 117997, Moscow, Russia.
*** Corresponding author. Institute for Physiology and Pathophysiology, University of Heidelberg, 69120, Heidelberg, Germany.
E-mail addresses: rozov1511@gmail.com (A.V. Rozov), olegpodgorny@inbox.ru (O.V. Podgorny), belousov@fccps.ru (V.V. Belousov).
[1] These authors contributed equally.

https://doi.org/10.1016/j.redox.2023.102604
Received 2 November 2022; Received in revised form 11 December 2022; Accepted 7 January 2023
Available online 10 January 2023

1. Introduction

Action potential propagation and synaptic transmission are the central processes of neuronal computation. Even under basal conditions, when a strong stimulus is absent, these processes are highly energy consuming. Every synaptic event triggers neuronal usage of energy for restoring the resting membrane potential and the extrusion of cytosolic Ca^{2+}; biosynthesis and recycling of neurotransmitters; and synaptic vesicle loading and trafficking [1,2]. Neurons produce the bulk of their energy via oxidative phosphorylation in mitochondria [3] and therefore demand a sufficient supply of oxygen and intense operation of a plethora of interconnected redox-dependent metabolic pathways [4]. The intense redox-dependent metabolism in neurons is accompanied by the generation of a range of reactive oxygen species (ROS) [5,6]. Multiple antioxidant defense systems neutralize ROS to coordinate redox-dependent signaling and reduce their deleterious oxidizing effects on cellular components. Breaking the balance between ROS generation and neutralization results in oxidative stress, a state in which redox signaling is disrupted and biomolecules undergo oxidative damage [7,8]. Neurons have a large number of oxidative targets, but a relatively weak antioxidant defense system, and are therefore very vulnerable to oxidative stress [9,10]. Aging-related mental health problems as well as Alzheimer's disease, the most common neurodegenerative disorder in people aged 65 and older, are characterized by the appearance of neuronal oxidative stress markers such as products of lipid peroxidation, and deleterious oxidative modifications of proteins and nucleic acids [11–13].

Both aging-related dementia and Alzheimer's disease feature progressive learning and memory deficits. Learning and memory are vital brain functions and, at the cellular level, are known to depend on the ability of neurons to vary the efficacy of synaptic transmission in an activity-dependent manner. This property, referred to as synaptic plasticity, underlies accumulation, storage, and utilization of information about animal or human experiences in order to shape adequate behavioral and physiological reactions in response to changes in the environment and the internal state. Various neuronal activity patterns may induce different forms of synaptic plasticity, and changes in the efficacy of excitatory transmission may last from milliseconds, as in synaptic facilitation, to hours and days, as in long-term potentiation (LTP) [14]. Different forms of synaptic plasticity may overlap in an individual synaptic connection, and this overlap is considered a mechanism of neuronal computation [15].

It is currently assumed that dysregulation of redox homeostasis in the aging brain underlies the impairment of synaptic transmission and plasticity, which leads to a decrease in the computational ability of neurons and, as a result, to learning and memory deficits [16]. Although a causative role of neuronal oxidative stress in the development of cognitive aging and neurodegeneration is widely accepted, it has not yet been sufficiently proven, primarily because of the lack of tools for emulating isolated oxidative stress. Here, we employed a chemogenetic tool based on the flavoprotein D-amino acid oxidase (DAAO) (EC-1.4.3.3) from the yeast *Rhodotorula gracilis* [17] to emulate oxidative stress by triggering controlled synthesis of intraneuronal hydrogen peroxide (H_2O_2) [18–20], the most stable ROS, and investigated its acute effects on synaptic transmission.

2. Materials and methods

2.1. Construction of vectors for expression of DAAO, DAAO(R285A) and HyPer7

To express the recombinant flavoprotein D-amino acid oxidase (DAAO) (EC-1.4.3.3) from the yeast *Rhodotorula gracilis* [17], its inactive mutant DAAO(R285A) [21], and the ultrasensitive H_2O_2 biosensor HyPer7 [22] in neurons *in vitro* and *in vivo*, we created recombinant adeno-associated viral (AAV) vectors serotype DJ and 9, carrying the respective genetic constructs. The constructs *pAAV-CaMKII-RFP-p2A-DAAO-NES+(wpre-sv40)*, *pAAV-CaMKII-RFP--p2A-DAAO(R285A)-NES+(wpre-sv40)*, and *pAAV-CaMKII-HyPer7+(wpre-sv40)*, in which CaMKIIα = Ca^{2+}/calmodulin-dependent protein kinase II alpha promoter [23], RFP = red fluorescent protein, p2A = a self-cleaving peptide, NES = nuclear export signal, wpre = woodchuck hepatitis posttranscriptional regulatory element, and sv40 = Simian virus 40 enhancer, were created on the basis of the *pAAV-mDlx-GFP--Fishell-1* vector [24] (a gift from Gordon Fishell; Addgene plasmid #83900) by replacing a promoter and fusing the corresponding cDNAs in the same open read frame. *Escherichia coli* XL1-Blue strain (Evrogen, #CC001) was used for the cloning, maintenance, and propagation of plasmids. All manipulations were conducted between the *Mlu*I and *Hind*III restriction enzyme sites. *pAAV-CaMKIIa-mCherry* (a gift from Karl Deisseroth; Addgene plasmid #114469) and *pTagRFP-C* (Evrogen, #FP141) vectors were used as promoter and RFP sequence sources. The DAAO sequence with the NES signal on the 3′ end was obtained from the *pAAV-HyPer-DAAO-NES* vector [20] (a gift from Thomas Michel; Addgene plasmid #119164) and fitted after RFP through p2A peptide. The construct encoding the inactive DAAO(R285A) was created by partial replacement of the DAAO sequence in *pAAV-CaMKII-RFP-p2A-DAAO-NES+(wpre-sv40)* with the respective sequence from the construct (see below) containing the point mutation R285A. The HyPer7 sequence was obtained from the *pCS2+HyPer7* vector [22]. The created constructs were verified by restriction analysis with appropriate restriction enzyme sets and sequencing. Midipreps were prepared using the Plasmid Midiprep 2.0 kit (Evrogen, #BC124) according to the manufacturer's instructions. Then, the constructs were packaged into AAV viral particles at the Viral Core Facility of Shemyakin-Ovchinnikov Institute of Bioorganic Chemistry. The constructs were packaged either in AAV serotype DJ viral particles for *in vitro* experiments using primary neuronal cell cultures or in AAV serotype 9 viral particles for stereotactic injections in mice. The virus titers were 2.2E+12 viral genomes (VG)/mL for AAV2/DJ-CaMKIIα-RFP--p2A-DAAO-NES; 1.4E+12 VG/mL for AAV2/DJ-CaMKIIα-RFP-p2A--DAAO(R285A)-NES; 8.3E+12 VG/mL for AAV2/DJ-CaMKIIα-HyPer7; 3.0E+12 VG/mL for AAV2/9-CaMKIIα-RFP-p2A-DAAO-NES; 5.5E+12 VG/mL for AAV2/9-CaMKIIα-RFP-p2A-DAAO(R285A)-NES; and 1.1E+12 VG/mL AAV2/9-CaMKIIα-HyPer7.

To evaluate the applicability of D-amino acids for chemogenetic generation of H_2O_2 in HeLa Kyoto cells, we created the plasmid constructs *pAAV-CMV-RFP-p2A-DAAO-NES+(wpre-sv40)*, *pAAV-CMV-RFP-p2A-DAAO(R285A)-NES+(wpre-sv40)*, and *pAAV-CMV-HyPer7+(wpre-sv40)* by promoter replacement in the plasmid constructs as described above, using the *pTagRFP-C* vector as a sequence source of the cytomegalovirus (CMV) promoter.

Arg^{285} plays a crucial role in stabilization of D-amino acids at the active site of DAAO and thus in the redox activity of the enzyme. The point mutation R285A significantly increases the Michaelis constant K_m for D-amino acids and decreases turnover number [21], rendering DAAO (R285A) almost inactive with mostly unaltered structure. To introduce a R285A mutation into DAAO, we amplified two fragments using two pairs of primers: (i) Hy-EcoR-F (5′-aatagaattcgccaccatggagatggcaagccagcag-3'; forward primer for introducing a R285A mutation into DAAO) and R285-R (5′- ctctcctggcgggtgccaggccaacgttatgtctcagcac -3'; reverse primer for introducing a R285A mutation into DAAO), and (ii) R285-F (5′-cgttggcctggcacccgccaggagaggagga-3'; forward primer for introducing a R285A mutation into DAAO) and DAAO-Hind-R (5′-gtacaagcttttagctctccctagctgcgcc -3'; reverse primer for introducing a R285A mutation into DAAO); and *pAAV-HyPer-DAAO-NES* plasmid as a template. This was followed by another round of polymerase chain reaction, using the PCR fragments obtained and Hy-Ecor-F and DAAO-Hind-R primers to produce the complete construct. The final product was inserted into the *pAAV-HyPer-DAAO-NES* vector between *Eco*RI and *Hind*III restriction enzyme sites to create the *pAAV-HyPer-DAAO(R285A)* vector.

2.2. Mice

Experiments were carried out using C57Bl/6J mice (The Jackson Laboratory, #000664, RRID: IMSR_JAX:000664). Mice were maintained in groups (3–4 mice per cage) in the animal facility of Shemyakin-Ovchinnikov Institute of Bioorganic Chemistry. Mice were housed in an ambient temperature 22–24 °C with a 12-hr light/dark cycle and had *ad libitum* access to food and water. All manipulations with animals were conducted according to the European Convention for the Protection of Vertebrate Animals used for Experimental and other Scientific Purposes (1986, ETS 123) and approved by the Institutional Animal Care and Use Committee (approval no. 331).

2.3. Embryonic mouse hippocampal neurons

E17 mouse embryos of both genders were collected on ice, and brains were isolated and placed in ice-cold 10 mM HEPES-Na (PanEco, #F134) supplemented Hanks' balanced salt solution without Mg^{2+} and Ca^{2+} (HBSSΔCaMg) (ThermoFisher Scientific, #14175095). The hemispheres were separated from meninges, and the hippocampi were carefully extracted and washed twice with fresh ice-cold HBSSΔCaMg. Hippocampi were incubated in HBSSΔCaMg supplemented with 0.025% trypsin (ThermoFisher Scientific, #27250018) and DNaseI (5 units/mL) (ThermoFisher Scientific, #90083) for 15 min at 37 °C. Trypsin activity was inhibited with full MEM: Minimum Essential Media (Sigma-Aldrich, #M3024) containing B27 supplement (ThemroFisher Scientific, #17504044), 5% fetal bovine serum (FBS) (Biosera, #FB-1001), GlutaMax (ThemroFisher Scientific, #35050061), 10 mM HEPES-Na, 6 g/L glucose, 2.2 g/L sodium bicarbonate, 100 units/mL of penicillin, and 100 μg/mL of streptomycin (PanEco, #A063). Neurons were gently resuspended in 1 mL of full MEM and filtered using the Falcon® 40 μm Cell Strainer (Corning, #352340). Cells were counted using a hemocytometer, and 1.5×10^5 cells in 150 μL of full MEM were plated on a 35 mm glass-bottom dish (SPL Life Sciences, #100350) pre-coated with poly-D-lysine (Sigma-Aldrich, #A-003-M). Dishes with plated cells were incubated for 40 min at 37 °C in ambient atmosphere with 5% CO_2. Then, 2 mL of full MEM was added to each dish for further cultivation. Once every two-three days, 30% of the culture medium was replaced with fresh full MEM.

2.4. Transduction of embryonic mouse hippocampal neurons

On the 5th day after plating, primary neuronal cell cultures were transduced with AAV vectors. Prior to the addition of the AAV vectors, half (1 mL) of the culture medium (conditioned MEM) was collected and stored at 4 °C until necessary. Fresh full MEM and AAV stock solutions were mixed, and 1 mL of the mixture was added into dishes with plated cells to achieve the final concentration of AAV vectors at 10^{10} VG/mL. On the following day, the culture medium was fully substituted with a mixture (1:1) of fresh full MEM and conditioned MEM. Transduced primary neuronal cell cultures were imaged 2 weeks later.

2.5. Culture and transfection of HeLa cell line

HeLa Kyoto (EMBL collection, gender: F, RRID: CVCL_1922) were cultured in DMEM/F12 (Gibco, #12634-010) supplemented with 10% fetal calf serum (FCS) (Biosera, #FB-1001), GlutaMAX (1:100) and Penicillin-Streptomycin mixture (1:100) (Gibco, #15140-122) at 37 °C in ambient atmosphere with 5% CO_2. HeLa Kyoto cell culture was tested for mycoplasma contamination using MycoReport kit (Evrogen, #MR001) according to manufacturer's guidelines. For real-time imaging, HeLa Kyoto cells were seeded in 35 mm glass-bottom dishes (SPL Life Sciences, #100350) and cultured in 2 mL of DMEM/F12 supplemented with 10% FCS, GlutaMAX (1:100) and Penicillin-Streptomycin mixture (1:100) at 37 °C in ambient atmosphere with 5% CO_2. Cells were transfected with a mixture of 1 μg DNA and 3 μL FuGene HD reagent (Promega, #E2311) in 100 μL Opti-MEM (Gibco, #15140-122) per dish.

2.6. Live-cell fluorescent imaging

Live-cell fluorescent imaging of primary neuronal cell cultures and HeLa Kyoto cells was carried out using a Nikon ECLIPSE Ti2-E epi-fluorescent microscope equipped with a SPECTRA X light engine and a Photometrics BSI camera. Prior to imaging, culture media were replaced with the pre-warmed Krebs-Ringer solution (140 mM NaCl, 5 mM KCl, 2 mM $CaCl_2$, 1 mM $MgCl_2$, 10 mM D-glucose, 10 mM HEPES; pH 7.4) or HBSS supplemented with 10 mM HEPES-Na for primary neuronal cell cultures or HeLa Kyoto cells, respectively. The fluorescent signals of HyPer7 and RFP were acquired using Nikon CFI S Plan Fluor LWD 20X (NA 0.7) and Plan Apo λ 40x (NA 0.95) objectives. Live cell imaging was carried out using Nikon NIS-Elements software. HyPer7 was sequentially excited at 395 nm and 470 nm, and its fluorescence was acquired within the spectral range 500–530 nm. RFP was excited at a 555 nm, and its fluorescence was acquired within the spectral range 580–610 nm. We performed time-lapse imaging with 20 s interframe intervals to measure changes in fluorescence of HyPer7 in neurons and HeLa cells expressing DAAO or DAAO(R285A) (RFP positive cells) in response to addition of the DAAO substrates and 200 μM H_2O_2 (Sigma-Aldrich, # 95321). Substances were added in a middle of the 20 s interframe interval. Images were captured in 5–6 randomly selected fields of view for each dish.

2.7. DAAO substrates

We evaluated several nonpolar, polar, aromatic, and basic D-amino acids including a non-proteinogenic amino acid D-isomer (norvaline) as potent substrates for DAAO activation. We examined the kinetics of H_2O_2 production in the cytosol of HeLa Kyoto cells upon treatment with the following D-amino acids: D-Cysteine (D-Cys, Fluorochem, #049424), D-Norvaline (D-Nva, Sigma-Algrich, #851620), D-Serine (D-Ser, Sigma-Algrich, #S4250), D-Threonine (D-Thr, Sigma-Algrich, #T8250), D-Lysine monohydrochloride (D-Lys, Sigma-Algrich, #L5876), D-Alanine (D-Ala, Sigma-Algrich, #A7377), D-Phenylalanine (D-Phe, Sigma-Algrich, #P1751), and D-Methionine (D-Met, Sigma-Algrich, #M9375).

2.8. Stereotaxic viral vector delivery

AAV vectors were delivered to CA1 area of the hippocampus by standard stereotaxic surgery [23,25]. Briefly, 6-week-old male mice were deeply anesthetized with 3% isoflurane (Baxter, #5AGG9621) in an induction chamber using a low-flow anesthesia system (SomnoSuite, Kent Scientific). Then, mice were placed onto the heating pad of the stereotaxic apparatus (digital stereotaxic instrument, Stoelting Co). Anesthesia was maintained by delivery of 1.5% isoflurane via inhalation mask. Body temperature was controlled by a rectal thermometer. Prior to incision, 0.25% bupivacaine (Ozon, #LP-003590) was injected subcutaneously (the total dose was less than 8 mg/kg) at the site of incision for local analgesia. After the skin on the mouse head was incised, connective tissue was removed using sterile cotton buds, and the surface of the skull was dried to facilitate identification of the bregma. The skull surface was aligned in anteroposterior and mediolateral directions. AAV vectors were injected into the intermediate/ventral hippocampus using a Hamilton microsyringe 75RN 5 μL (Hamilton, #7634-01) equipped with a 33-gauge needle via holes drilled in the skull at the stereotaxic coordinates: −3.3 mm anteroposterior, ±3.4 mm mediolateral (both hemispheres), and −3.9/-3.6/-3.3 mm dorsoventral relative to the bregma [25,26]. At each point in the dorsoventral axis, 400 nL of the AAV vector solution was delivered at 200 nL/min. After the wound was closed, animals were placed into individual cages for recovery. For analgesia, mice were intraperitoneally injected with ketoprofen (5 mg/kg) (Sandoz, #N013942/01) immediately after surgery, and again 24 and 48 h after surgery. Mice recovered for at least 2 weeks after

surgery. The recovery period also enabled sufficient expression of DAAO, DAAO(R285A) and HyPer7 to be reached.

2.9. Preparation of acute brain slices

Mice that received AAV vector intrahippocampal injections were deeply anesthetized with 3% isoflurane and decapitated, and the brains were isolated from skulls. Transverse hippocampal 300 μm slices were prepared from the isolated brains. The slicing chamber contained an oxygenated ice-cold solution composed of (in mM): K-Gluconate, 140; N-(2-hydroxyethyl) piperazine-N′-ethanesulfonic acid (HEPES), 10; Na-Gluconate, 15; ethylene glycol-bis (2-aminoethyl)-N, N, N′, N′-tetra-acetic acid, 0.2; and NaCl, 4 (pH 7.2). Slices were incubated for 30 min at 35 °C before being stored at room temperature in artificial cerebrospinal fluid (ACSF) containing (in mM): NaCl, 125; NaHCO3, 25; KCl, 2.5; NaH2PO4, 1.25; MgCl2, 1; CaCl2, 2; and D-glucose, 25; bubbled with 95% O2 and 5% CO2.

2.10. Confocal imaging of acute slices

Acute brain slices were imaged using an inverted Nikon A1 confocal microscope. To replicate the conditions used for electrophysiological recordings, we created a perfusion chamber based on a 35 mm glass-bottom dish (SPL Life Sciences, #101350) to provide incubation of brain slices in ACSF saturated with carbogen (95% O2 and 5% CO2). Acute brain slices were placed on pieces of nylon fishing line (diameter 0.2 mm) to allow ACSF to flow past the slice surface adjacent to the glass bottom of the dish. To avoid slice movement during perfusion, they were secured by a metallic grid with nylon fibers. Fluorescent signals of HyPer7 and RFP were acquired from a single optical plane at the approximate depth of 20 μm from the slice surface adjacent to the glass bottom via a Nikon Plan Apo λ 40x (NA 0.95) objective using Nikon NIS-Elements software. HyPer7 was sequentially excited by 405 nm and 488 nm laser lines, and its fluorescence was acquired within the spectral range 500–530 nm. RFP was excited by a 561 nm laser line, and its fluorescence was acquired within the spectral range 570–620 nm. We performed time-lapse imaging with 20 s interframe intervals to measure changes in the fluorescence of HyPer7 in neurons expressing DAAO or DAAO(R285A) (RFP positive neurons) in response to the addition of 2 mM D-Nva at 10 min and 200 μM H_2O_2 at 40 min after the beginning of capturing. Images were captured from slices obtained from 3 mice injected with the AAV vector encoding DAAO and 3 mice injected with the AAV vector encoding DAAO(R285A).

2.11. Detection of the neuronal marker NeuN

To confirm expression of DAAO in neurons, three mice received intrahippocampal injections of the AAV vector AAV2/9-CaMKIIα-RFP-p2A-DAAO-NES. Two weeks later, mice were deeply anesthetized by an intraperitoneal injection of a mixture of tiletamine/zolazepam/xylazine at doses of 40/40/20 mg/kg. Then, anesthetized mice underwent transcardiac perfusion with 0.01 M phosphate buffered saline (PBS, pH 7.4) followed by cold 4% paraformaldehyde in PBS (pH 7.4) according to standard procedures. Brains were extracted from skulls and postfixed overnight at 4 °C. On the following day, the brains were washed with PBS, and the hemispheres were sliced sagittally with a Leica VT1200S vibratome (Leica-Microsystems). Free floating slices (thickness of 50 μm) with AAV infection detected by fluorescence of RFP were further processed for immunofluorescent staining with the anti-NeuN antibody. Slices were initially permeabilized in 4% Triton X-100 (Sigma-Aldrich, #T8787) in PBS for 1 h followed by blocking in 5% goat serum (Sigma-Aldrich, #G9023) in PBS containing 0.2% Triton X-100 for 1 h. Then, slices were incubated with the primary rabbit anti-NeuN polyclonal antibody (1:1000, Abcam, #ab104225) diluted in the blocking solution overnight at room temperature. On the following day, slices were washed three times in PBS (5 min each) and stained with the secondary goat anti-rabbit IgG (H + L) antibody conjugated with Alexa Fluor 488 (1:500) (Thermo Fisher Scientific, #A11036) for 2 h at room temperature. The antibody was dissolved in the blocking solution supplemented with 2 μg/ml DAPI (Sigma-Aldrich, #D9542) for staining cell nuclei. Stained brain slices were washed three times in PBS (5 min each), attached to gelatin-coated glass-slides, mounted in Fluorescence Mounting Medium (DAKO, #S3023) and covered with coverslips. Preparations were imaged using an inverted Nikon A1 confocal microscope. Z-stacks of the CA1 area of the hippocampus were acquired via a Nikon Plan Apo λ 40x (NA 0.95) objective using Nikon NIS-Elements software. The step size of the Z-stack was 1 μm. To avoid overlap of fluorescent signals between neighbor channels, we sequentially (plane by plane) scanned individual channels, exciting DAPI, NeuN-Alexa Fluor 488 and RFP by laser lines 405 nm, 488 nm and 561 nm, respectively.

2.12. Image analysis

The image processing Fiji software (RRID:SCR_002285) was used to create quantitative datasets for determining the kinetics of the HyPer7 ratiometric signal in primary neuronal cell cultures, HeLa cells, and acute slices. Widefield and confocal image files in the nd2 format were imported into the Fiji software using Bio-formats importer. All files contained images acquired in three channels: red – RFP, blue – HyPer7 excited at either 395 or 405 nm, and green – HyPer7 excited at either 470 or 488 nm. The background was subtracted straightaway using the Sliding paraboloid item with a Rolling ball radius of 50.0 pixels. Cell bodies with RFP and HyPer7 fluorescence were selected using the wand tool utility. The selections were used as regions of interest (ROIs) and added to the ROI manager of Fiji software. Then, channels were split, mean values of fluorescence for ROI were measured, and digitized fluorescence datasets for each ROI in green and blue channels were separately exported using the Multi measure tool. For each time point and an individual ROI, the fluorescence value in the green channel (referred here as $F490_{i,t}$) was divided by the value in the blue channel (referred here as $F400_{i,t}$) to determine the HyPer7 ratio:

$$R_{i,t} = \frac{F490_{i,t}}{F400_{i,t}}, \quad (1)$$

where i is a given ROI, and t is a given time point. The mean value of the HyPer7 ratio for an individual ROI was determined for the time interval prior to addition of the DAAO substrates (from 0 to 2 min for primary neuronal cell cultures and HeLa Kyoto cells, and from 0 to 10 min for acute brain slices). Then, HyPer7 ratios for a given ROI were normalized to this mean value to determine the kinetics of the HyPer7 ratiometric signal. Averaging individual kinetic curves provided a resultant response of cells expressing DAAO or its inactive form DAAO(R285A) to the addition of DAAO substrates and treatment with 200 μM H_2O_2.

2.13. Acute slice electrophysiology

During experiments, slices were continuously perfused with ACSF. Patch electrodes were pulled from hard borosilicate capillary glass (Sutter Instruments flaming/brown micropipette puller). Electrodes for the postsynaptic pyramidal cells were filled with a solution consisting of (in mM): Cs-gluconate, 100; CsCl, 40; HEPES, 10; NaCl, 8; MgATP, 4; MgGTP, 0.3; phosphocreatine, 10 (pH 7.3 with CsOH).

CA1 pyramidal cells were visually identified using IR-video microscopy. Expression of wild type or mutant DAAO in the neurons was confirmed by the presence of RFP. Whole-cell recordings from these neurons were taken at room temperature (23–25 °C) in voltage-clamp mode using a HEKA EPC-10 amplifier (List Elektronik) with a sampling rate of 100 μs and filtered at 3 kHz. GABAergic synaptic transmission was blocked by continuous presence of the $GABA_A$ receptor antagonist SR95531 (10 μM). The effects of different concentrations of D-amino acids on EPSC amplitudes were tested upon stimulation of inputs

to the apical dendrites at the holding potential −70 mV. In LTP experiments, EPSCs were evoked from two independent inputs, to the basal and apical dendrites, with two patch pipettes used as stimulating electrodes located in *str. oriens* and *str. radiatum*, respectively.

Input to the basal dendrites was used as the control pathway, the apical dendrite input was potentiated. Prior to and after LTP induction, neurons were held at −70 mV, and both inputs were stimulated every 6 s. LTP was evoked by pairing depolarization of the postsynaptic pyramidal cell to 0 mV for 3 min with stimulation of the inputs to the apical dendrites every 1.5 s. The measured amplitudes were normalized to the mean baseline EPSCs before pairing. Neurons whose access resistance changed by more than 15% during the experiment were excluded from the analysis.

2.14. Statistics

Statistical analyses of changes of the HyPer7 ratio in primary neuronal cell cultures and acute brain slices upon addition of DAAO substrates was performed using R version 4.2.0 in RStudio 2022.02.2 Build 485 (RStudio Team). Since the HyPer7 ratio deviated from normality and sphericity, we used nonparametric ANOVA-type statistics (ATS) using the nparLD package [27]. Experiments were analyzed in the framework of an F1-LD-F1 design. The dependent variable was the HyPer7 ratio. The independent factors were substrate concentration combined with presence of mutation in DAAO and treatment (baseline (no treatment), treatment with a DAAO substrate, treatment with H_2O_2). Substrate concentration combined with presence of mutation was analyzed as the "between-subject" factor, treatment was analyzed as the "within-subject" factor. Statistical significance of changes of the HyPer7 ratio in primary neuronal cell cultures and acute brain slices upon addition of DAAO substrates was assessed in neurons expressing DAAO vs neurons expressing DAAO(R285A) by the post hoc Dunn's test using the PMCMRplus package (https://CRAN.R-project.org/package=PMCMRplus). The details of statistical analysis are given in the figure legends.

The statistical significance of LTP for mice that received viral vectors either with DAAO or DAAO(R285A) under different experimental conditions was assessed by comparing normalized EPSC amplitudes in the paired and unpaired pathways recorded in the period 20–30 min after LTP induction using SigmaStat 4.0 software (RRID: SCR_010285). For cross-comparison effects in neurons expressing DAAO and DAAO(R285), the values of relative potentiation calculated by subtraction of the normalized EPSC amplitudes in the unpaired pathway from those in the paired pathway were used. The time window of statistical assessment was the same: 20–30 min after LTP induction. The details of statistical analysis are given in the figure legends.

3. Results

3.1. Chemogenetic production of intraneuronal hydrogen peroxide

Initially, we validated the chemogenetic tool in primary neuronal cell cultures from the embryonic mouse hippocampus. Cultured neurons were co-transduced with pairs of adeno-associated viral (AAV) vectors carrying constructs for CaMKIIα (Ca^{2+}/calmodulin-dependent protein kinase II alpha) promoter-driven expression of DAAO (AAV2/DJ-CaMKIIα-RFP-p2A-DAAO-NES; RFP = red fluorescent protein, p2A = a self-cleaving peptide, NES = nuclear export signal) or its inactive mutant DAAO(R285A) [21] (AAV2/DJ-CaMKIIα-RFP-p2A-DAAO(R285A)-NES) with the ultrasensitive ratiometric H_2O_2 biosensor HyPer7 [22] (AAV2/DJ-CaMKIIα-HyPer7). In our initial experiments, we treated transduced neurons with D-alanine (D-Ala) that was widely used as a DAAO substrate in previous studies [18–20]. The key advantage of D-Ala as a DAAO substrate is that oxidative deamination converts it into pyruvate that is readily metabolized by the cell [28]. In DAAO-expressing neurons, extracellular application of D-Ala significantly elevated neuronal H_2O_2 levels in a concentration dependent manner over several minutes as determined by changes in HyPer7 fluorescence (Fig. S1, Supplementary Materials). No change in the HyPer7 ratio occurred after addition of D-Ala to neurons expressing inactive DAAO(R285A) (Fig. S1, Supplementary Materials). We assumed D-Ala to be a suitable substrate for DAAO for electrophysiological recordings of CA1 pyramidal neurons in acute brain slices, however this failed. At concentrations above 2 mM which markedly elevated the HyPer7 ratio in cultured neurons, D-Ala itself reduced the amplitude of excitatory postsynaptic currents (EPSCs) evoked by stimulation of Schaffer collaterals (Fig. S2, Supplementary Materials). Therefore, we evaluated several other D-amino acids for use as the substrate for chemogenetic H_2O_2 production (Fig. S3, Supplementary Materials). D-norvaline (D-Nva) was chosen because it evoked similar levels of HyPer7 oxidation at much lower concentrations than D-Ala and is a non-proteinogenic amino acid D-isomer. Therefore, even if D-Nva undergoes enzymatic racemization, it should not interfere with cellular amino acid metabolism.

Similarly to D-Ala, extracellular application of D-Nva significantly elevated neuronal H_2O_2 levels in cultured neurons expressing DAAO in a concentration dependent manner, and did not change the fluorescence of HyPer7 in cultured neurons expressing DAAO(R285A) (Fig. 1; Fig. S4, Supplementary Materials). D-Nva at the concentration of 10 mM exerted almost complete oxidation of HyPer7, rendering it insensitive to further addition of H_2O_2 (Fig. 1B and C; Fig. S4, Supplementary Materials). D-Nva at the concentration of 2 mM elicited a half-maximal response similar to that when cultured neurons were treated with 10 mM D-Ala (Figs. S1B–C, Supplementary Materials). In a previous study [18], DAAO was shown to produce intracellular H_2O_2 at concentrations that do not exceed the 50–100 nM range notwithstanding treatment of cells with millimolar concentrations of D-Ala. Low intracellular concentrations of molecular oxygen seem to limit the rate of the D-amino acid deamination mediated by DAAO [18]. The equality of responses of HyPer7 upon treatment of cultured neurons with 2 mM D-Nva or 10 mM D-Ala ensures that the concentration of chemogenetically generated intracellular H_2O_2 was within the physiological nanomolar range [18,22,29]. Therefore, for experiments in acute brain slices, we used 2 mM D-Nva.

Next, we examined chemogenetic production of intracellular H_2O_2 and its physiological effects on acute hippocampal slices. For this purpose, the same pairs of genetic constructs packaged in AAV serotype 9 vectors were stereotactically injected into the CA1 region of the mouse hippocampus (Fig. 2A). Two weeks later, necessary for sufficient expression of DAAO, DAAO(R285A) and HyPer7, the brains were dissected for slice preparation and subsequent *ex vivo* experiments. Acute transverse brain slices were either imaged by confocal microscopy to confirm chemogenetically induced generation of H_2O_2 in CA1 pyramidal neurons, or were used for electrophysiological recordings (Fig. 2B).

Since dissociated cultured neurons obtained from embryonic hippocampus may differ from mature hippocampal cells in terms of amino acid transport and metabolism, we carried out verification of chemogenetically induced production of H_2O_2 in acute brain slices as well. As observed in the primary neuronal cultures, addition of 2 mM D-Nva to the artificial cerebrospinal fluid (ACSF) significantly elevated H_2O_2 level in CA1 pyramidal neurons expressing DAAO, and did not change the fluorescence of HyPer7 in CA1 pyramidal neurons expressing DAAO (R285A) (Fig. 2C–E). Although the magnitudes of the HyPer7 ratio in response to D-Nva and H_2O_2 were smaller than those observed in primary neuronal cultures, live confocal imaging confirmed the applicability of recombinant DAAO as a chemogenetic tool, and its inactivated form as an appropriate control to study the physiological effects of substrate-induced intracellular H_2O_2 generation in acute brain slices.

To confirm expression of DAAO in hippocampal CA1 pyramidal neurons, we delivered the AAV vector AAV2/9-CaMKIIα-RFP-p2A-DAAO-NES to the hippocampus of three additional mice. Two weeks later, mice were sacrificed, and their brains were processed for detection of the neuronal cell marker NeuN. Confocal imaging confirmed

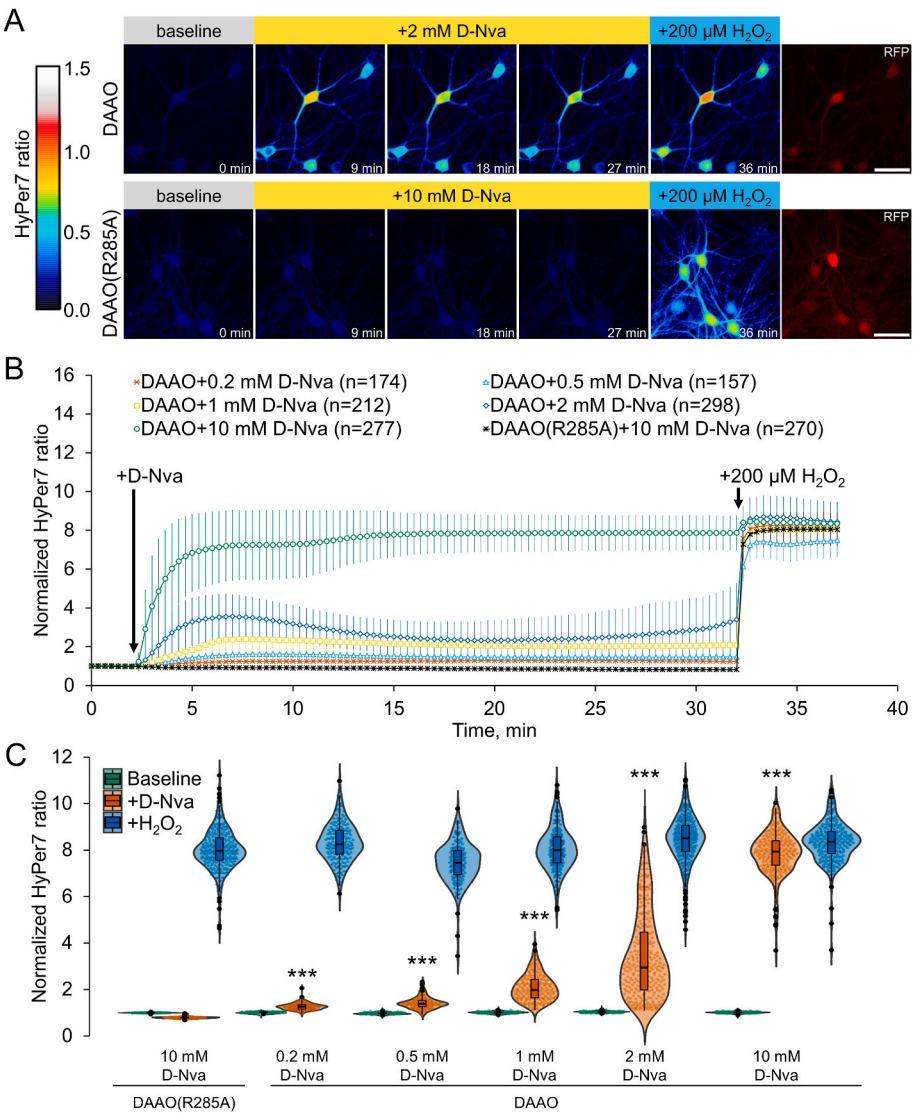

Fig. 1. Expression of DAAO and substrate-dependent production of H_2O_2 in cultured neurons. **A.** Widefield real-time ratiometric fluorescent images of cultured neurons expressing either DAAO or DAAO(R285A) (RFP-positive neurons). Primary neuronal cell cultures were co-transduced by AAV vector pairs carrying constructs for expression of DAAO or DAAO (R285A) with the HyPer7 sensor. 30 min after D-Nva addition, cultured neurons were treated with 200 μM H_2O_2 to reveal full oxidation of HyPer7 sensor. Scale bars: 50 μm. See also Video S1, Supplementary Materials, that demonstrates changes in HyPer7 ratio in cultured neurons with either DAAO or DAAO(R285A) upon addition of D-Nva and H_2O_2. **B.** Time-course of HyPer7 ratio changes in neurons with either DAAO or DAAO(R285A) upon addition of various concentrations of D-Nva followed by treatment with 200 μM H_2O_2. HyPer7 ratios at individual time points are normalized to the average HyPer7 ratio prior to the addition of D-Nva. Data are shown as mean ± standard deviation (SD). **C.** Distributions of normalized HyPer7 ratios at the timepoints 2 min (baseline), 32 min (D-Nva), and 37 min (H_2O_2). Statistical analysis revealed significant elevation of the HyPer7 ratio in response to treatment of neurons expressing DAAO with various concentrations of D-Nva vs. treatment of neurons expressing DAAO(R285A) with 10 mM D-Nva (nonparametric ANOVA-type statistics with a mixed model design ($F_{4.7,\infty} = 471.3$, $p < 1e\text{-}4$) followed by post hoc Dunn's test with Holm's adjustment for multiple comparison, $^{***}p < 0.001$). This figure presents data of a single experimental replicate. An independent replicate of the same experiment is presented in Fig. S4, Supplementary Materials.

expression of DAAO in the NeuN-immunopositive CA1 pyramidal neurons (Fig. 2F).

3.2. Action of chemogenetically produced intraneuronal hydrogen peroxide on synaptic transmission and plasticity

Treatment of acute hippocampal slices with 2 mM D-Nva did not have any effect on the amplitudes of evoked EPSCs in CA1 pyramidal neurons expressing DAAO(R285A) (Fig. 3). This observation confirmed that D-Nva itself does not affect basal synaptic transmission. Addition of 2 mM D-Nva slightly decreased the amplitudes of evoked EPSCs in CA1 neurons with DAAO but did not alter the paired-pulse ratio (Fig. 3). The latter observation indicated that chemogenetically produced H_2O_2 had no effect on the probability of synaptic vesicular release.

Next, we evaluated the effects of chemogenetically-generated H_2O_2 on induction and maintenance of long-term potentiation (LTP) in CA1 pyramidal neurons expressing DAAO or DAAO(R285A). LTP is a type of activity dependent synaptic plasticity that causes long-lasting enhancement of synaptic transmission and is assumed to underlie some forms of learning. To assess effects of intraneuronal oxidative stress on LTP, acute brain slices were incubated in ACSF containing 2 mM D-Nva for at least 20 min prior to the beginning of electrophysiological recording to achieve stable levels of the H_2O_2 production. Then, in the ACSF containing 2 mM D-Nva, we performed whole-cell voltage clamp recordings in CA1 pyramidal neurons expressing either DAAO or DAAO(R285A) (Fig. 4A) with independent stimulation of inputs to the apical and basal dendrites. After recording baseline EPSCs, LTP was induced by pairing low-frequency presynaptic stimulation (0.67 Hz) of the input to the apical dendrites with postsynaptic depolarization to 0 mV for 3 min [30] (LTP pathway), while the basal dendrites remained unstimulated (control pathway). EPSC amplitudes at potentiated synapses increased both in neurons expressing DAAO and DAAO(R285A) (Fig. 4B and C). However, the maximal level of LTP in neurons expressing DAAO was significantly smaller than that in neurons expressing DAAO(R285A) (Fig. 4D). Moreover, EPSCs amplitudes at potentiated synapses of DAAO expressing cells declined to near baseline level within 30 min, while EPSCs in neurons expressing DAAO(R285) remained potentiated throughout the recording period (Fig. 4B–D).

Since the AAV vectors infected a large area of the hippocampus including the dentate gyrus and CA3, DAAO could be expressed in presynaptic neurons as well. To verify that the observed LTP decline was not due to the effects of H_2O_2 on presynaptic neurons, we loaded neurons expressing DAAO or DAAO(R285A) with 1 mM D-Nva through the patch pipette. Similarly to the exogenous application of D-Nva, LTP was expressed normally in CA1 pyramidal neurons with DAAO(R285A) and suppressed in DAAO-expressing cells (Fig. 5A–C).

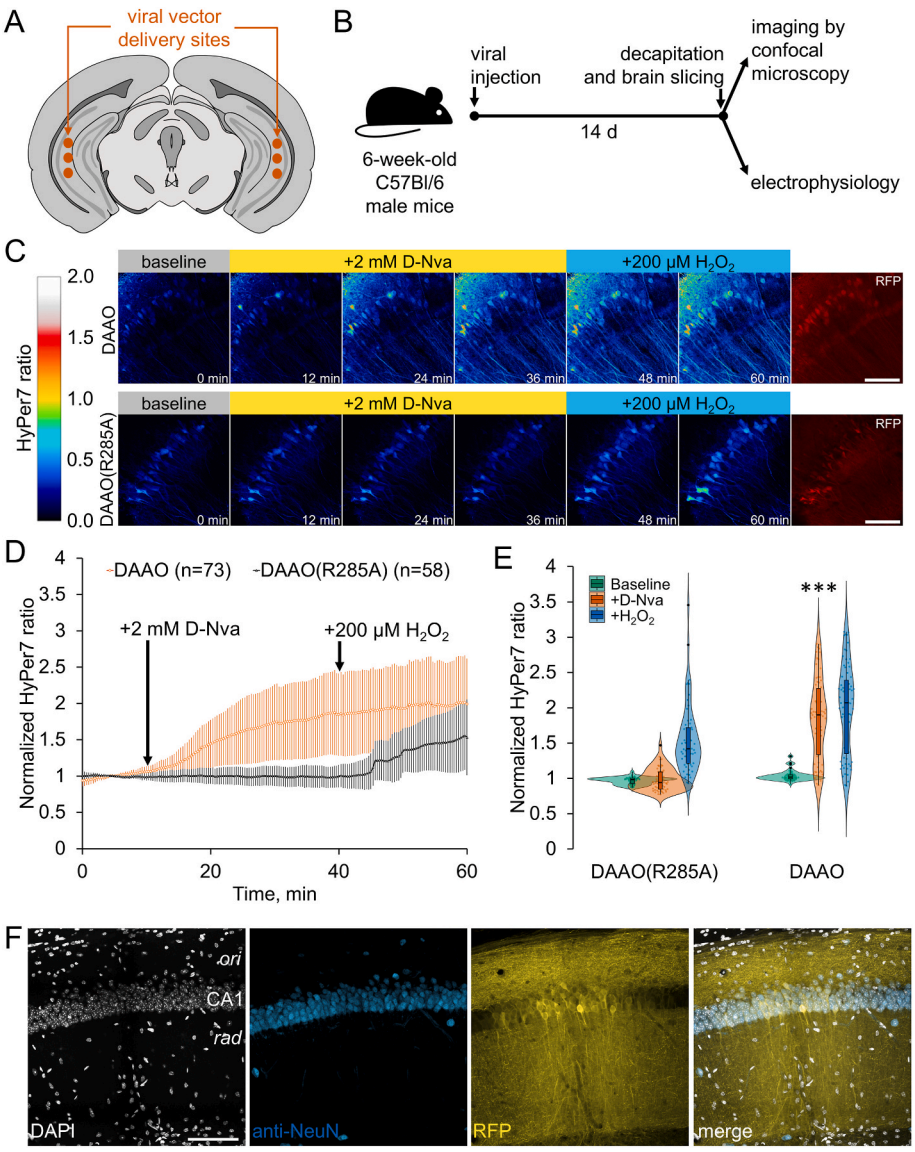

Fig. 2. Expression of DAAO and substrate-dependent production of H_2O_2 in acute brain slices. **A.** Site of viral vector delivery in the hippocampal CA1 area. The stereotaxic coordinates: −3.3 mm anteroposterior, ±3.4 mm mediolateral (both hemispheres), and −3.9/-3.6/-3.3 mm dorsoventral relative to the bregma. **B.** Outline of the experimental design. **C.** Confocal ratiometric fluorescent time-lapse images of CA1 pyramidal neurons expressing either DAAO or DAAO(R285A) (RFP-positive neurons). Mice received intrahippocampal injections of AAV vector pairs carrying constructs for coexpression of DAAO or DAAO(R285A) with the HyPer7 sensor. Images were acquired from a single optical plane at the approximate depth of 20 μm under the slice surface. Scale bars: 100 μm. **D.** Time-course of HyPer7 ratio changes in CA1 pyramidal neurons with either DAAO or DAAO(R285A) upon addition of 2 mM D-Nva to ACSF followed by supplementation of 200 μM H_2O_2. HyPer7 ratios at individual time points were normalized to the average HyPer7 ratio prior to the addition of D-Nva. Data are shown as mean ± SD. **E.** Distributions of normalized HyPer7 ratios at the timepoints 10 min (baseline), 40 min (D-Nva), and 60 min (H_2O_2). Statistical analysis revealed significant elevation of the HyPer7 ratio in response to treatment of CA1 pyramidal neurons expressing DAAO with 2 mM D-Nva vs. treatment of CA1 pyramidal neurons expressing DAAO(R285A) with 2 mM D-Nva (nonparametric ANOVA-type statistics with a mixed model design ($F_{1,\infty} = 100.3$, $p < 1e\text{-}4$) followed by post hoc Dunn's test, $^{***}p < 0.001$). Panels **D** and **E** present combined data from three mice with neurons expressing DAAO and three mice with neurons expressing DAAO(R285A). **F.** Expression of DAAO in NeuN-positive pyramidal cells in the hippocampal CA1 area. The panel shows maximum intensity projection of the hippocampal CA1 area. CA1: CA1 area; *rad*: *str. radiatum*; *ori*: *str. oriens*. Scale bar: 100 μm.

Deamination of D-Nva by DAAO produces not only H_2O_2 but also 2-oxovaleric acid, a D-Nva derivate, and ammonia (NH_3/NH_4^+). According to the catalytic cycle of the reaction catalyzed by DAAO all products should be produced at equimolar concentrations [17,31]. Recombinant DAAO produces H_2O_2 in the host cell cytoplasm at concentrations below 100 nM [18]. Given that the basal level of cytosolic H_2O_2 is within the 2–3 nM range [32], DAAO produces H_2O_2 at physiologically relevant levels. At the same time, the basal levels of ammonia in the brain and the cerebrospinal fluid have been estimated starting at 100 μM [33]. Obviously, relative to this value, a possible DAAO-mediated increase in ammonia concentration is negligible. The concentration of 2-oxovaleric acid in blood serum was found to be approximately 60 nM [34]. Hence, DAAO-mediated production of 2-oxovaleric acid in equimolar concentrations to H_2O_2 can potentially exhibit physiological effects. To prove that the observed LTP suppression is triggered by chemogenetically generated H_2O_2 and not by the D-Nva derivate, we tested the effect of intracellularly loaded 2-oxovaleric acid on LTP induction. At the concentration of 100 μM, considerably more than expected from DAAO activity, 2-oxovaleric acid did not cause any effect on LTP level in the neurons expressing DAAO confirming the major role of chemogenetically produced H_2O_2 in the LTP suppression (Fig. 5D).

4. Discussion

Here, we reveal that chemogenetically generated intraneuronal H_2O_2 elicits acute effects on synaptic plasticity. We report that intraneuronally produced H_2O_2 does not alter the probability of neurotransmitter release from presynaptic terminals but significantly reduces LTP in CA1 pyramidal neurons. The latter observation enables us to argue that intraneuronal H_2O_2 causes alterations of synaptic plasticity that may manifest in the form of cognitive impairment before the onset of evident neurodegeneration. Therefore, recombinant yeast DAAO is a unique tool for studying the early stages of oxidative stress-induced pathogenesis in which the function, but not the integrity and viability of neurons is affected. Targeting DAAO to defined brain areas, cell populations, or subcellular compartments and varying the dosage of the DAAO substrate and the time course of its delivery enable a large spectrum of oxidative stress emulation scenarios to be created. The combination of this chemogenetic tool with electrophysiological recordings provides a powerful platform for screening potential antioxidants effective against neuronal oxidative stress. Yet another application of this chemogenetic tool is the identification of early markers of neuronal oxidative stress.

In our study, we aimed to elucidate the effects of chemogenetically

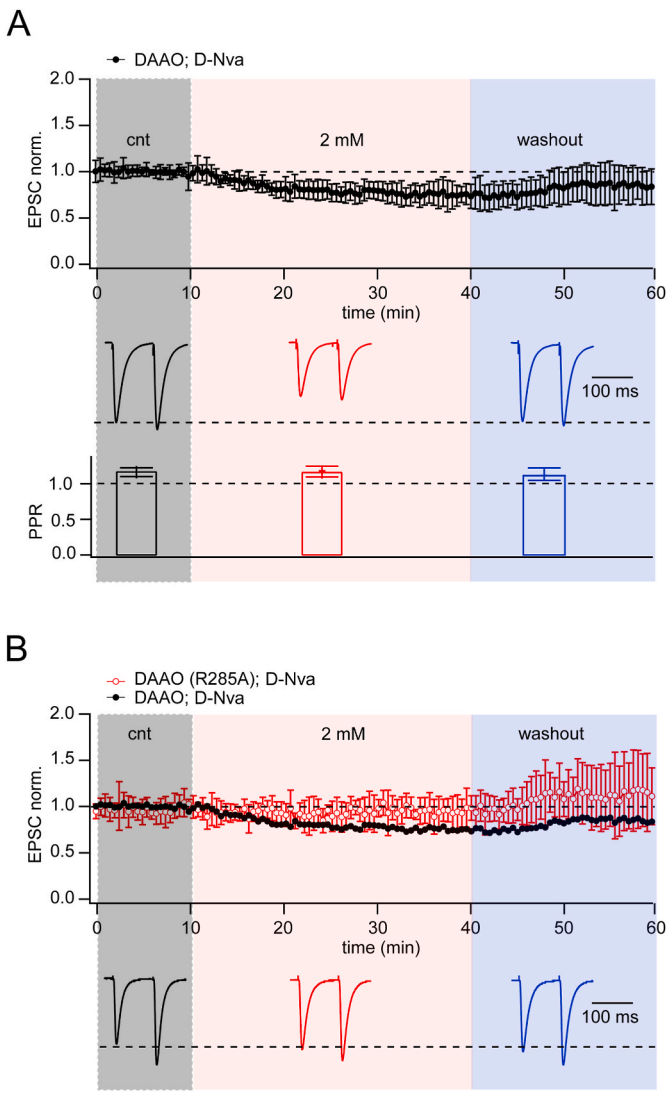

Fig. 3. D-Nva application slightly decreases EPSC amplitudes in CA1 pyramidal neurons expressing DAAO but does not change synaptic efficacy at excitatory synapses of CA1 pyramidal neurons expressing DAAO(R285A). **A.** Effect of extracellular application of D-Nva on synaptic efficacy at excitatory synapses of CA1 pyramidal cells expressing DAAO. The scatter plot represents normalized EPSC amplitudes recorded prior to D-Nva application (gray box), in the presence of D-Nva (2 mM; pink box) and during subsequent washout of the drug (8 cells from 2 mice). Traces underneath show averaged EPSCs recorded during the last 5 min of every step of the experiment. Bar histograms compare paired pulse ratios of EPSCs (PPR) under control conditions, in the presence of, and after washout of D-Nva. D-Nva at this concentration causes small, but significant reduction of EPSC amplitudes. **B.** Effect of extracellular application of D-Nva on synaptic efficacy at excitatory synapses of CA1 pyramidal cells expressing DAAO(R285A). The scatter plot represents normalized EPSC amplitudes recorded prior to D-Nva application (gray box), in the presence of D-Nva (2 mM; pink box) and during subsequent washout of the drug (5 cells from 1 mouse). The effect of D-Nva on EPSCs in neurons expressing active DAAO is plotted with black symbols for comparison. Note that D-Nva does not have any statistically significant effect on the amplitude of postsynaptic responses in cells expressing DAAO(R285A). (For interpretation of the references to color in this figure legend, the reader is referred to the Web version of this article.)

produced H_2O_2 on synaptic transmission and plasticity because of the following reasons. First, LTP as a form of cellular memory formation is often used to assess the physiological action of many biologically active compounds. Second, it was unknown whether DAAO when expressed in neurons is able to produce H_2O_2 in amounts essential for the appearance of any acute effects on neuronal cell function. Third, acute effects of exogenous H_2O_2 on LTP in the contexts of intact or impaired neuronal redox states have been revealed previously in several studies [35–39]. Hence, examination of the DAAO-mediated generation of intraneuronal H_2O_2 in a well-established experimental paradigm validates the chemogenetic tool.

One of the key findings in our study is that chemogenetically produced intraneuronal H_2O_2 reduces LTP in CA1 pyramidal neurons at the single cell level. Previously, the effects of H_2O_2 on LTP in acute brain slices were found to vary from inhibitory to facilitating depending on the H_2O_2 concentration and a preceding neuronal redox state [35–39]. The most commonly used approaches for evaluating the effects of H_2O_2 on synaptic transmission were the application of exogenous H_2O_2 or manipulation of the cellular antioxidant defense systems [35–39]. However, these approaches have low specificity for the following reasons. First, the observed alterations in LTP may reflect network effects of oxidative stress. Second, under these conditions, oxidative stress is induced not only in neurons but also in all other brain cell types, including astrocytes and microglia, which are known to modulate the LTP via independent signaling pathways [40–44]. Third, when H_2O_2 is applied exogenously, it is impossible to dissect the contributions of intracellular and extracellular oxidative imbalances to the observed alterations in LTP. Fourth, manipulation of the cellular antioxidant defense systems globally deregulates redox-dependent metabolism and signaling, and this may contribute to impairment of LTP independent of H_2O_2 production. Application of this DAAO-based chemogenetic tool enables more realistic oxidative stress conditions to be created. This is critically important for studying the pathogenesis of cognitive aging, identifying early markers of neuronal oxidative stress, and screening potential antioxidants effective against neuronal oxidative stress.

LTP is a complex phenomenon, and although it has received the attention of many research groups for almost half a century, there is no consensus on the mechanism of induction and/or maintenance of LTP. It is known that LTP at Shaffer collateral synapses requires calcium influx via the N-methyl-D-Aspartate receptor (NMDAR) [45], which promotes CaMKII-dependent phosphorylation [46]. The GluA1 subunit of the α-amino-3-hydroxy-5-methyl-4-isoxazolepropionic acid receptor (AMPAR) channels is also known to play a critical role in LTP induction [47], but there is still debate as to whether phosphorylation of the GluA1-containing AMPARs present in the synapse leads to increased responses or whether induction protocols somehow activate lateral transport of extrasynaptic GluA1-containing channels to potentiated synapses [48,49]. H_2O_2 can interfere with any of these vital steps in LTP induction, it can decrease NMDAR function, change phosphorylation rate, and finally affect intracellular transport. Thus, in order to better understand the effect of H_2O_2 on long-term plasticity, it is necessary to consider all these steps, which can only be done in a separate study. Oxidative stress can be caused by inflammation, severe life stress, and various neurodegenerative diseases. All these pathological conditions are also accompanied by a decrease in LTP. However, it was not entirely clear whether the influence on LTP should be attributed to the production of reactive oxygen species or to other ongoing pathobiological processes. We believe that the main values of this study are: a direct demonstration that intracellular H_2O_2 production can suppress LTP, and the presentation of a new chemogenetic tool that will facilitate further study of the role of oxidative stress in the pathogenesis of neural networks.

In the cell, H_2O_2 is primarily produced though spontaneous or enzyme-catalyzed dismutation of superoxide anion formed due to the activities of the electron transport chain, NADPH oxidases, and some proteins of the endoplasmic reticulum and the proxisomes [50]. H_2O_2 plays dual role in the cell depending on its intracellular concentration. Fluctuations of H_2O_2 around basal level promote signaling function primarily via modifications of redox-sensitive cysteine and methionine residues in proteins [50,51]. In this regard, the use of the chemogenetic tool based on DAAO is advantageous because it allows for modulation of

normal redox signaling at defined sites and time points. At concentrations much higher than basal, H_2O_2 exhibits toxic effects on cellular components primarily through secondary oxidizing agents generated by conversion of H_2O_2 in several metabolic pathways. H_2O_2 participates in myeloperoxidase-mediated peroxidation of Cl^- with formation a strong oxidizing agent hypochlorous acid (HOCl) [52] and in the Fenton reaction with ferrous ions to produce the extremely reactive hydroxyl radical [53]. Importantly, oxidative damage of cellular components can occur without H_2O_2. For instance, superoxide anion, if not metabolized by a superoxide dismutase, can either produce the highly toxic peroxynitrite anion ($ONOO^-$) when it reacts with available nitric oxide ($^{\bullet}NO$) [54] or induce lipid peroxidation in the protonated form ($HO_2^{\bullet}$) [55]. Therefore, chemogenetic emulation of intracellular oxidative stress using DAAO is unable to replicate certain aspects of oxidative damage.

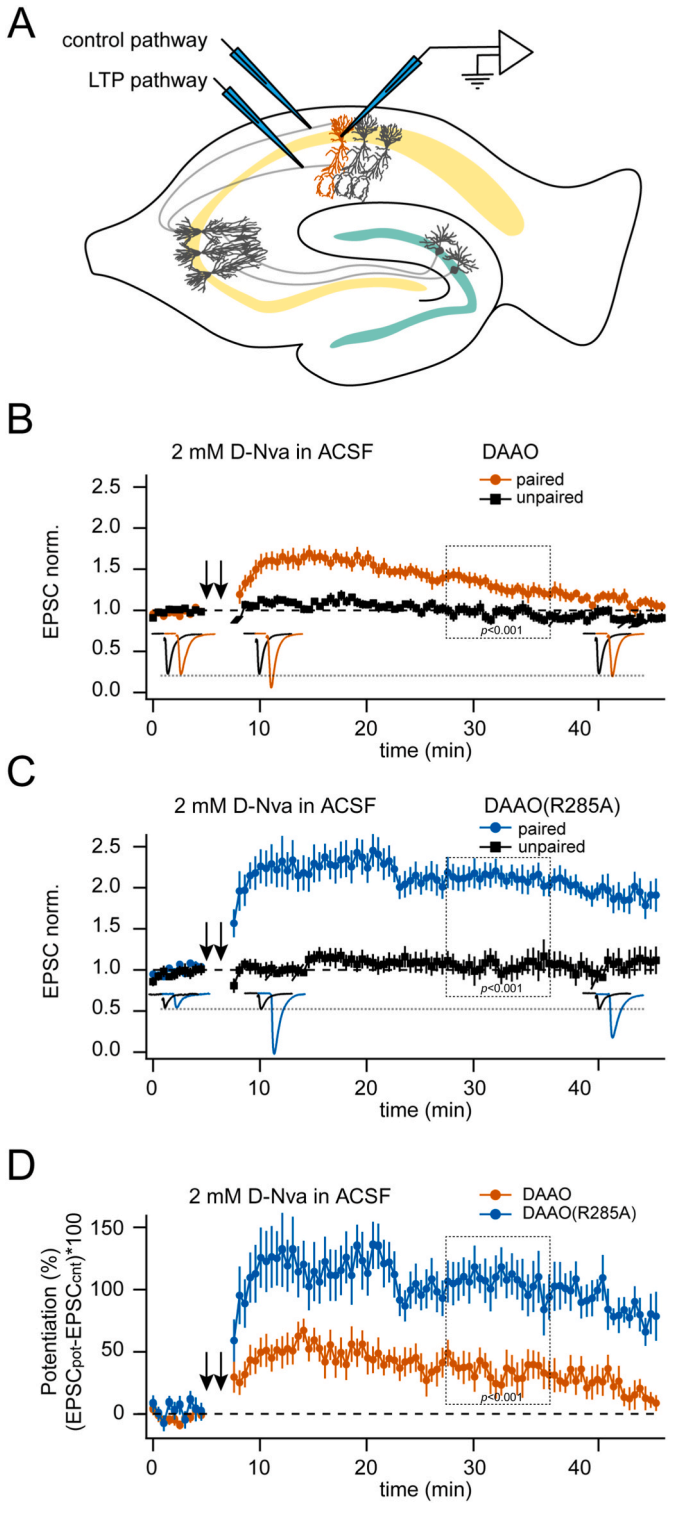

(caption on next column)

Fig. 4. The effect of chemogenetically produced H_2O_2 on LTP in CA1 pyramidal neurons upon exogenous application of D-Nva. **A.** Schematic representation of horizontal hippocampal slice with position of stimulation and patch-clamp electrodes. **B.** D-Nva application significantly reduces the level of LTP in CA1 neurons expressing DAAO. Median values measured in the interval 20–30 min after potentiation in the paired and unpaired pathways were 1.14 vs. 0.94 (12 cells from 8 mice; $p < 0.001$ Wilcoxon Test). Normalized EPSC amplitudes recorded from RFP-positive CA1 pyramidal neurons with stimulation of inputs from CA3 pyramidal cells to basal (black symbols) and apical (brown symbols) dendrites. The LTP induction is indicated by the two arrows. **C** D-Nva application does not cause reduction of LTP in CA1 neurons expressing DAAO (R285A) (medians paired vs. unpaired: 2.14 vs. 0.98; 10 cells from 7 mice; $p < 0.001$ Wilcoxon Test). The same as in (**B**), data from the paired input to the apical dendrites and the corresponding traces are shown in blue. **D.** Comparison of LTP in neurons expressing DAAO (brown symbols) and DAAO(R285A) (blue symbols) recorded in the presence of extracellular D-Nva (LTP medians DAAO (12 cells from 8 mice) vs DAAO(R285A) (10 cells from 7 mice): 15% vs. 97%; p < 0.001 Mann-Whitney Test). D-Nva was applied at least 20 min prior to the beginning of the experiments and was present throughout the recording time. The plotted data were obtained by subtraction of the normalized EPSC values measured at the unpaired synapse from those obtained at paired inputs. The insets underneath the scatter plots show the averaged representative traces from a cell recorded before pairing, during the first 10 min after pairing and during the last 10 min of the recording. The color code of traces from paired and unpaired inputs is the same as on the scatter plots. All data in this figure are shown as mean ± standard error of mean (SEM). Dashed line frames show the datasets used for statistical analysis. (For interpretation of the references to color in this figure legend, the reader is referred to the Web version of this article.)

Another key finding of our study is that D-Ala, a commonly used DAAO substrate for chemogenetic H_2O_2 generation, is not ideal for experiments on the brain. The key advantage of D-Ala was the generation of a byproduct that is rapidly metabolized by the cell, pyruvate. Moreover, as DAAO generates nanomolar amounts of H_2O_2, pyruvate is also generated in the nanomolar range, which is 2–3 orders of magnitude lower than the intracellular Pyr pool [56]. However, we revealed that D-Ala itself affects EPSCs evoked by stimulation of Schaffer collaterals. Therefore, we tested several other substrates and selected D-Nva for further experiments because it lacked the unwanted effects of D-Ala, and in addition was more effective as a DAAO substrate.

Mammalian brain has endogenous D-amino acid metabolism. This metabolism is primarily related to D-serine (D-Ser), although some other D-amino acids were also demonstrated to exhibit physiological effects in the brain (reviewed in Ref. [57]). D-Ser is synthetized and degraded in both neurons and astrocytes. It functions as the N-methyl-D-Aspartate receptor co-agonist at the glycine binding site [58–60]. D-Ser is degraded by endogenous mammalian DAAO present in several regions of the mammalian brain. Interestingly, DAAO was identified by the specific antibody in the rat hippocampus [61], but there was no DAAO activity detected in the mouse hippocampus by high-performance liquid chromatographic assay [62]. Yeast DAAO displays much higher activity than mammalian DAAO, having a turnover number for D-Ala as substrate several dozen times higher than mammalian DAAO [17,63,64]. Therefore, in our experiments on acute hippocampal slices, the application of the yeast DAAO-based chemogenetic tool could potentially interfere with endogenous D-amino acid metabolism. But in fact, we observed normal expression of LTP in neurons expressing inactive DAAO (R285A) upon treatment with D-Nva and in neurons expressing DAAO upon treatment with 2-oxovaleric acid. These observations indicate that, even if the chemogenetic tool interferes with endogenous D-amino acid

metabolism, effects of this interference are negligible.

Our study reveals that chemogenetically induced intraneuronal oxidative stress reduces LTP, but does not investigate this on the behavioral level. There are numerous studies that correlate impairment of LTP with some forms of the learning and memory deficit in behavioral tests [36,40,65–67]. We believe that impairment of synaptic plasticity

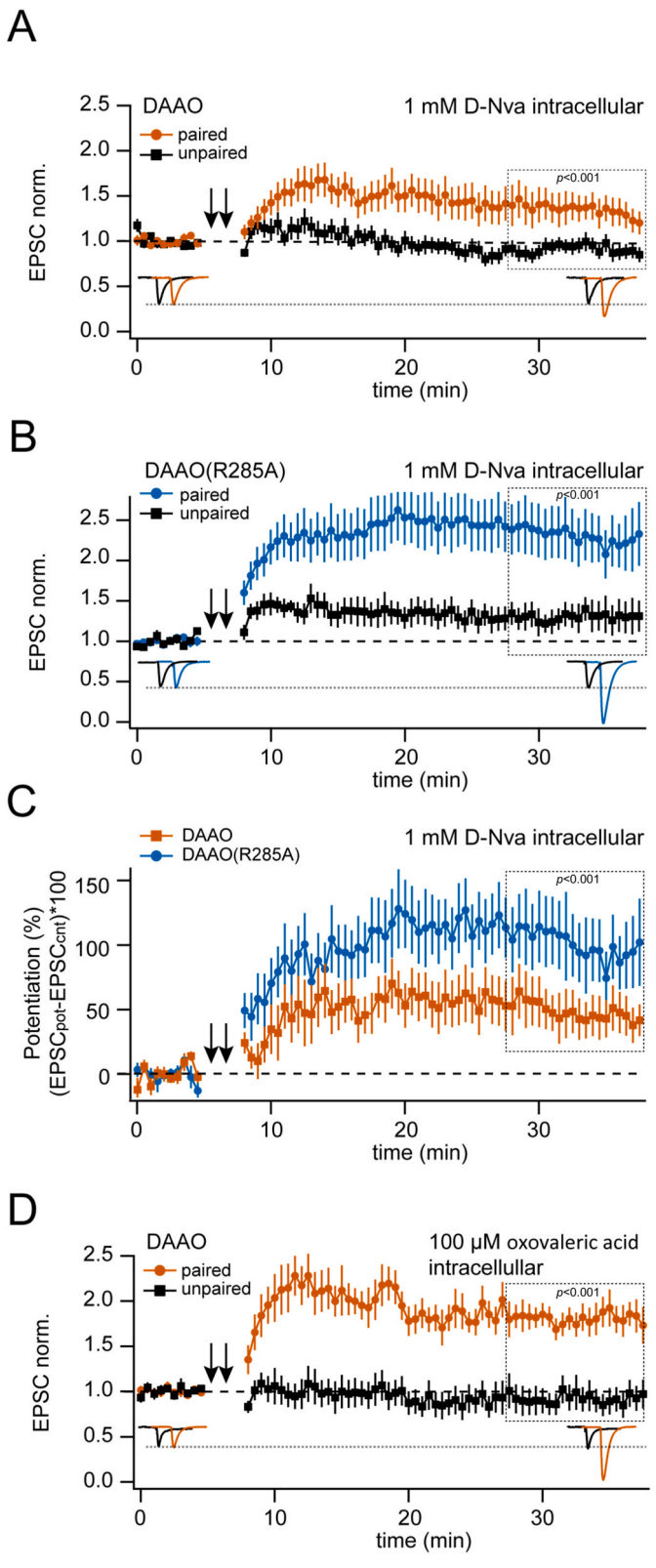

(caption on next column)

Fig. 5. The effect of chemogenetically produced H_2O_2 on LTP in CA1 pyramidal neurons upon intraneuronal loading of D-Nva. **A.** D-Nva intracellular loading significantly reduces the level of LTP in CA1 neurons expressing DAAO. Median values measured in the interval 20–30 min after potentiation in the paired and unpaired pathways were 1.24 vs. 0.9 (11 cells from 5 mice; $p < 0.001$ Wilcoxon Test). Input to the apical dendrites was potentiated (brown symbols), input to the basal dendrites was used as the control pathway. **B.** D-Nva intracellular loading does not change expression of LTP in CA1 neurons expressing DAAO (R285A) (medians paired vs. unpaired: 1.87 vs. 1.24; 10 cells from 9 mice; $p < 0.001$ Wilcoxon Test). The same as in (**A**), data from paired input to the apical dendrites and the corresponding traces are shown in blue. **C.** Comparison of LTP in neurons expressing DAAO (brown symbols) and DAAO(R285A) (blue symbols) recorded in neurons loaded with D-Nva via a patch electrode (LTP medians DAAO vs DAAO(R285A): 35% vs. 89%; $p < 0.001$ Mann-Whitney Test). The plotted data were obtained by subtraction of the normalized EPSC values measured at the unpaired synapse from those obtained at paired inputs. **D.** Intracellular loading of 2-oxovaleric acid does not change expression of LTP in CA1 neurons expressing DAAO (medians paired vs. unpaired: 1.74 vs. 0.96; 6 cells from 5 mice; $p < 0.001$ Wilcoxon Test). Input to the apical dendrites was potentiated (brown symbols), input to the basal dendrites was used as control pathway. D-Nva or 2-oxovaleric acid was loaded at least 20 min prior to the beginning of the experiments and was present throughout the recording time. The insets underneath the scatter plots show the averaged representative traces from one cell recorded before pairing and during the last 10 min of the recording. The color code of traces from paired and unpaired inputs is the same as on the scatter plots. All data in this figure are shown as mean ± SEM. Dashed line frames show the datasets used for statistical analysis. (For interpretation of the references to color in this figure legend, the reader is referred to the Web version of this article.)

induced by the chemogenetic production of intraneuronal H_2O_2 may be manifested as a learning and memory deficit. The previous successful application of the DAAO-based chemogenetic tool for modelling cardiac dysfunction *in vivo* [20] and the reported ability of D-amino acids to penetrate the blood-brain barrier (BBB) [68–70] allow us to speculate that this tool can be used for creating the oxidative stress state in the brain *in vivo*. This will help us to answer the question on the role of neuronal oxidative stress in the development of cognitive aging and neurodegeneration. If *in vivo* experiments reveal that chemogenetically-induced oxidative stress does drive behavioral impairments, evident neuronal cell death, and other features of aging related brain pathologies, DAAO may be a promising tool for creating more proper animal models emulating cognitive aging and the early stages of neurodegeneration. In this case, targeting DAAO to specific neuronal cell types in the animal brain may be used for modeling of the most common neurodegenerative disorders such as Alzheimer's disease and Parkinson's disease.

In the previous study, to create oxidative stress in the heart *in vivo*, rats with DAAO in cardiomyocytes were fed with D-Ala via drinking water [20]. However, employment of the chemogenetic tool based on DAAO in the brain *in vivo* may represent a challenge. Although D-amino acids have been shown to cross the BBB [68–70], there is no evidence of their transport into neurons in the literature. Our *in vitro* and *ex vivo* experiments, in which the BBB is absent or disrupted, demonstrate that D-amino acids readily enter into neurons. However, in the brain with an intact BBB, astrocytes can metabolize D-amino acids, decreasing or even interrupting their transport from blood plasma to neurons. This can render the DAAO-based cheogenetic tool ineffective for the purposes it has been created. Therefore, delivery of D-amino acids via intravenous or intraperitoneal injections, or by cannulation of the brain ventricles may help overcome this challenge, allowing for employment of this chemogenetic tool *in vivo*.

5. Conclusions

In sum, we report the application of recombinant yeast DAAO as a chemogenetic tool for emulating controlled and isolated neuronal

oxidative stress on the cellular level. Our results demonstrate that chemogenetically induced intraneuronal oxidative stress reduces LTP at single cell level and the LTP decline is caused solely by H_2O_2 and not by other products of the DAAO-mediated deamination of D-Nva. This chemogenetic tool may help to address a range of earlier unsolved questions regarding the roles of ROS-dependent signaling in normal brain functioning and the contribution of oxidative stress to the pathogenesis of cognitive aging and the early stages of neurodegeneration. A combination of this DAAO-based chemogenetic tool with electrophysiological recordings represents a powerful approach for screening potential neuroprotective drugs.

Ethics approval

All manipulations with animals were conducted according to the European Convention for the Protection of Vertebrate Animals used for Experimental and other Scientific Purposes (1986, ETS 123) and approved by the Institutional Animal Care and Use Committee of Shemyakin-Ovchinnikov Institute of Bioorganic Chemistry (approval no. 331).

Availability of data and materials

Further information and requests for resources and reagents should be directed to and will be fulfilled by the corresponding author, Dr. Oleg Podgorny (olegpodgorny@inbox.ru). Plasmids generated in this study are available from the corresponding author, Dr. Oleg Podgorny (olegpodgorny@inbox.ru), upon request. All primary quantitative data presented in this paper have been deposited as Excel and Origin files at Mendeley Data (https://doi.org/10.17632/68mfprpk2p.1) and are publicly available as of the date of publication. Original microscopy image data sets reported in this paper will be shared by the corresponding author, Dr. Oleg Podgorny (olegpodgorny@inbox.ru), upon request.

Funding

Creating genetic constructs and validating the DAAO-mediated generation of H_2O_2 in primary neuronal cell cultures and acute brain slices were funded by the Russian Science Foundation (RSF) grant 20-15-00280(to O.V.P.), testing of the DAAO substrates was funded by the Ministry of Science and Higher Education of the Russian Federation grant no. 075-15-2019-1789 to the Center for Precision Genome Editing and Genetic Technologies for Biomedicine, electrophysiological recordings were funded by the RSF grant 22-15-00293 (to A.V.R.), and electrophysiological data analysis was funded by the DFG grant RO 3062/2-1 (to A.V.R).

Author's contributions

V.V.B., O.V.P., and A.V.R. designed experiments, A.L.K., D.J., G.M.S., D.I.M., Y.A.B., A.A.M., L.F.M., R.A.S., and V.A.S. performed and analyzed experiments, O.V.P., and A.V.R. interpreted results, V.V.B., O.V.P., and A.V.R. wrote the manuscript. All authors read and approved the final manuscript.

Declaration of competing interest

The authors declare that they have no known competing financial interests or personal relationships that could have appeared to influence the work reported in this paper.

Data availability

Data will be made available on request.

Acknowledgements

We thank Ekaterina Potekhina for methodological advice.

Appendix A. Supplementary data

Supplementary data to this article can be found online at https://doi.org/10.1016/j.redox.2023.102604.

References

[1] J.J. Harris, R. Jolivet, D. Attwell, Synaptic energy use and supply, Neuron 75 (2012) 762–777, https://doi.org/10.1016/j.neuron.2012.08.019.
[2] S. Li, Z.-H. Sheng, Energy matters: presynaptic metabolism and the maintenance of synaptic transmission, Nat. Rev. Neurosci. 23 (2022) 4–22, https://doi.org/10.1038/s41583-021-00535-8.
[3] C.N. Hall, M.C. Klein-Flugge, C. Howarth, D. Attwell, Oxidative phosphorylation, not glycolysis, powers presynaptic and postsynaptic mechanisms underlying brain information processing, J. Neurosci. 32 (2012) 8940–8951, https://doi.org/10.1523/JNEUROSCI.0026-12.2012.
[4] S. Özugur, L. Kunz, H. Straka, Relationship between oxygen consumption and neuronal activity in a defined neural circuit, BMC Biol. 18 (2020) 76, https://doi.org/10.1186/s12915-020-00811-6.
[5] C. Quijano, M. Trujillo, L. Castro, A. Trostchansky, Interplay between oxidant species and energy metabolism, Redox Biol. 8 (2016) 28–42, https://doi.org/10.1016/j.redox.2015.11.010.
[6] C.C. Winterbourn, Reconciling the chemistry and biology of reactive oxygen species, Nat. Chem. Biol. 4 (2008) 278–286, https://doi.org/10.1038/nchembio.85.
[7] H. Sies, On the history of oxidative stress: concept and some aspects of current development, Current Opinion in Toxicology 7 (2018) 122–126, https://doi.org/10.1016/j.cotox.2018.01.002.
[8] H. Sies, C. Berndt, D.P. Jones, Oxidative stress, Annu. Rev. Biochem. 86 (2017) 715–748, https://doi.org/10.1146/annurev-biochem-061516-045037.
[9] J.N. Cobley, M.L. Fiorello, D.M. Bailey, 13 reasons why the brain is susceptible to oxidative stress, Redox Biol. 15 (2018) 490–503, https://doi.org/10.1016/j.redox.2018.01.008.
[10] R. Dringen, P.G. Pawlowski, J. Hirrlinger, Peroxide detoxification by brain cells, J. Neurosci. Res. 79 (2005) 157–165, https://doi.org/10.1002/jnr.20280.
[11] K.J. Barnham, C.L. Masters, A.I. Bush, Neurodegenerative diseases and oxidative stress, Nat. Rev. Drug Discov. 3 (2004) 205–214, https://doi.org/10.1038/nrd1330.
[12] J.K. Andersen, Oxidative stress in neurodegeneration: cause or consequence? Nat Med 10 (2004) https://doi.org/10.1038/nrn1434. S18–S25.
[13] W. Dröge, H.M. Schipper, Oxidative stress and aberrant signaling in aging and cognitive decline, Aging Cell 6 (2007) 361–370, https://doi.org/10.1111/j.1474-9726.2007.00294.x.
[14] A. Citri, R.C. Malenka, Synaptic plasticity: multiple forms, functions, and mechanisms, Neuropsychopharmacology 33 (2008) 18–41, https://doi.org/10.1038/sj.npp.1301559.
[15] L.F. Abbott, W.G. Regehr, Synaptic computation, Nature 431 (2004) 796–803, https://doi.org/10.1038/nature03010.
[16] A. Kumar, B. Yegla, T.C. Foster, Redox signaling in neurotransmission and cognition during aging, Antioxidants Redox Signal. 28 (2018) 1724–1745, https://doi.org/10.1089/ars.2017.7111.
[17] L. Pollegioni, B. Langkau, W. Tischer, S. Ghisla, M.S. Pilone, Kinetic mechanism of D-amino acid oxidases from Rhodotorula gracilis and Trigonopsis variabilis, J. Biol. Chem. 268 (1993) 13850–13857.
[18] M.E. Matlashov, V.V. Belousov, G. Enikolopov, How much H $_2$ O $_2$ is produced by recombinant D-amino acid oxidase in mammalian cells? Antioxidants Redox Signal. 20 (2014) 1039–1044, https://doi.org/10.1089/ars.2013.5618.
[19] R.E. Haskew-Layton, J.B. Payappilly, N.A. Smirnova, T.C. Ma, K.K. Chan, T. H. Murphy, H. Guo, B. Langley, R. Sultana, D.A. Butterfield, S. Santagata, M. J. Alldred, I.G. Gazaryan, G.W. Bell, S.D. Ginsberg, R.R. Ratan, Controlled enzymatic production of astrocytic hydrogen peroxide protects neurons from oxidative stress via an Nrf2-independent pathway, Proc. Natl. Acad. Sci. U.S.A. 107 (2010) 17385–17390, https://doi.org/10.1073/pnas.1003996107.
[20] B. Steinhorn, A. Sorrentino, S. Badole, Y. Bogdanova, V. Belousov, T. Michel, Chemogenetic generation of hydrogen peroxide in the heart induces severe cardiac dysfunction, Nat. Commun. 9 (2018) 4044, https://doi.org/10.1038/s41467-018-06533-2.
[21] G. Molla, D. Porrini, V. Job, L. Motteran, C. Vegezzi, S. Campaner, M.S. Pilone, L. Pollegioni, Role of arginine 285 in the active site of Rhodotorula gracilis d-amino acid oxidase, J. Biol. Chem. 275 (2000) 24715–24721, https://doi.org/10.1074/jbc.M908193199.
[22] V.V. Pak, D. Ezeriņa, O.G. Lyublinskaya, B. Pedre, P.A. Tyurin-Kuzmin, N. M. Mishina, M. Thauvin, D. Young, K. Wahni, S.A. Martínez Gache, A. D. Demidovich, Y.G. Ermakova, Y.D. Maslova, A.G. Shokhina, E. Eroglu, D.S. Bilan, I. Bogeski, T. Michel, S. Vriz, J. Messens, V.V. Belousov, Ultrasensitive genetically encoded indicator for hydrogen peroxide identifies roles for the oxidant in cell migration and mitochondrial function, Cell Metabol. 31 (2020) 642–653, https://doi.org/10.1016/j.cmet.2020.02.003, e6.

[23] T. Dittgen, A. Nimmerjahn, S. Komai, P. Licznerski, J. Waters, T.W. Margrie, F. Helmchen, W. Denk, M. Brecht, P. Osten, Lentivirus-based genetic manipulations of cortical neurons and their optical and electrophysiological monitoring in vivo, Proc. Natl. Acad. Sci. U. S. A. 101 (2004) 18206–18211, https://doi.org/10.1073/pnas.0407976101.

[24] J. Dimidschstein, Q. Chen, R. Tremblay, S.L. Rogers, G.-A. Saldi, L. Guo, Q. Xu, R. Liu, C. Lu, J. Chu, J.S. Grimley, A.-R. Krostag, A. Kaykas, M.C. Avery, M. S. Rashid, M. Baek, A.L. Jacob, G.B. Smith, D.E. Wilson, G. Kosche, I. Kruglikov, T. Rusielewicz, V.C. Kotak, T.M. Mowery, S.A. Anderson, E.M. Callaway, J. S. Dasen, D. Fitzpatrick, V. Fossati, M.A. Long, S. Noggle, J.H. Reynolds, D. H. Sanes, B. Rudy, G. Feng, G. Fishell, A viral strategy for targeting and manipulating interneurons across vertebrate species, Nat. Neurosci. 19 (2016) 1743–1749, https://doi.org/10.1038/nn.4430.

[25] A. Rozov, M. Rannap, F. Lorenz, A. Nasretdinov, A. Draguhn, A.V. Egorov, Processing of hippocampal network activity in the receiver network of the medial entorhinal cortex layer V, J. Neurosci. 40 (2020) 8413–8425, https://doi.org/10.1523/JNEUROSCI.0586-20.2020.

[26] K.B.J. Franklin, G. Paxinos, The Mouse Brain in Stereotaxic Coordinates, vol. 3, Elsevier, AP, Amsterdam, 2008.

[27] K. Noguchi, Y.R. Gel, E. Brunner, F. Konietschke, nparLD : an *R* software package for the nonparametric analysis of longitudinal data in factorial experiments, J. Stat. Software 50 (2012), https://doi.org/10.18637/jss.v050.i12.

[28] M. Dixon, K. Kleppe, d-amino acid oxidase II. Specificity, competitive inhibition and reaction sequence, Biochim. Biophys. Acta Nucleic Acids Protein Synth. 96 (1965) 368–382, https://doi.org/10.1016/0005-2787(65)90557-5.

[29] B.K. Huang, H.D. Sikes, Quantifying intracellular hydrogen peroxide perturbations in terms of concentration, Redox Biol. 2 (2014) 955–962, https://doi.org/10.1016/j.redox.2014.08.001.

[30] V. Jensen, K.M.M. Kaiser, T. Borchardt, G. Adelmann, A. Rozov, N. Burnashev, C. Brix, M. Frotscher, P. Andersen, Ø. Hvalby, B. Sakmann, P.H. Seeburg, R. Sprengel, A juvenile form of postsynaptic hippocampal long-term potentiation in mice deficient for the AMPA receptor subunit GluR-A, J. Physiol. 553 (2003) 843–856, https://doi.org/10.1113/jphysiol.2003.053637.

[31] L. Pollegioni, G. Molla, S. Sacchi, E. Rosini, R. Verga, M.S. Pilone, Properties and applications of microbial D-amino acid oxidases: current state and perspectives, Appl. Microbiol. Biotechnol. 78 (2008) 1–16, https://doi.org/10.1007/s00253-007-1282-4.

[32] O. Lyublinskaya, F. Antunes, Measuring intracellular concentration of hydrogen peroxide with the use of genetically encoded H2O2 biosensor HyPer, Redox Biol. 24 (2019), 101200, https://doi.org/10.1016/j.redox.2019.101200.

[33] A.J. Cooper, F. Plum, Biochemistry and physiology of brain ammonia, Physiol. Rev. 67 (1987) 440–519, https://doi.org/10.1152/physrev.1987.67.2.440.

[34] Z.J. Wang, K. Zaitsu, Y. Ohkura, High-performance liquid chromatographic determination of alpha-keto acids in human serum and urine using 1,2-diamino-4,5-methylenedioxybenzene as a precolumn fluorescence derivatization reagent, J Chromatogr 430 (1988) 223–231, https://doi.org/10.1016/s0378-4347(00)83157-6.

[35] C.A. Colton, L. Fagni, D. Gilbert, The action of hydrogen peroxide on paired pulse and long-term potentiation in the hippocampus, Free Radic. Biol. Med. 7 (1989) 3–8, https://doi.org/10.1016/0891-5849(89)90093-2.

[36] E. Gahtan, J.M. Auerbach, Y. Groner, M. Segal, Reversible impairment of long-term potentiation in transgenic Cu/Zn-SOD mice, Eur. J. Neurosci. 10 (1998) 538–544, https://doi.org/10.1046/j.1460-9568.1998.00058.x.

[37] A. Kamsler, M. Segal, Hydrogen peroxide modulation of synaptic plasticity, J. Neurosci. 23 (2003) 269–276, https://doi.org/10.1523/JNEUROSCI.23-01-00269.2003.

[38] A. Kamsler, M. Segal, Paradoxical actions of hydrogen peroxide on long-term potentiation in transgenic superoxide dismutase-1 mice, J. Neurosci. 23 (2003) 10359–10367.

[39] T.C. Pellmar, G.E. Hollinden, J.M. Sarvey, Free radicals accelerate the decay of long-term potentiation in field CA1 of Guinea-pig hippocampus, Neuroscience 44 (1991) 353–359, https://doi.org/10.1016/0306-4522(91)90060-2.

[40] L. Hösli, N. Binini, K.D. Ferrari, L. Thieren, Z.J. Looser, M. Zuend, H.S. Zanker, S. Berry, M. Holub, W. Möbius, T. Ruhwedel, K.-A. Nave, C. Giaume, B. Weber, A. S. Saab, Decoupling astrocytes in adult mice impairs synaptic plasticity and spatial learning, Cell Rep. 38 (2022), 110484, https://doi.org/10.1016/j.celrep.2022.110484.

[41] J. Sa de Almeida, M. Vargas, J. Fonseca-Gomes, S.R. Tanqueiro, R.F. Belo, C. Miranda-Lourenço, A.M. Sebastião, M.J. Diógenes, T.F. Pais, Microglial sirtuin 2 shapes long-term potentiation in hippocampal slices, Front. Neurosci. 14 (2020) 614, https://doi.org/10.3389/fnins.2020.00614.

[42] M.W. Sherwood, M. Arizono, C. Hisatsune, H. Bannai, E. Ebisui, J.L. Sherwood, A. Panatier, S.H.R. Oliet, K. Mikoshiba, Astrocytic IP $_3$ Rs: contribution to Ca $^{2+}$ signalling and hippocampal LTP: astrocytic IP $_3$ Rs: Ca $^{2+}$ signalling and LTP, Glia 65 (2017) 502–513, https://doi.org/10.1002/glia.23107.

[43] Y. Yang, W. Ge, Y. Chen, Z. Zhang, W. Shen, C. Wu, M. Poo, S. Duan, Contribution of astrocytes to hippocampal long-term potentiation through release of D-serine, Proc. Natl. Acad. Sci. U. S. A. 100 (2003) 15194–15199, https://doi.org/10.1073/pnas.2431073100.

[44] E.M. York, J. Zhang, H.B. Choi, B.A. MacVicar, Neuroinflammatory inhibition of synaptic long-term potentiation requires immunometabolic reprogramming of microglia, Glia 69 (2021) 567–578, https://doi.org/10.1002/glia.23913.

[45] J.Z. Tsien, P.T. Huerta, S. Tonegawa, The essential role of hippocampal CA1 NMDA receptor–dependent synaptic plasticity in spatial memory, Cell 87 (1996) 1327–1338, https://doi.org/10.1016/S0092-8674(00)81827-9.

[46] J. Lisman, The CaM kinase II hypothesis for the storage of synaptic memory, Trends Neurosci. 17 (1994) 406–412, https://doi.org/10.1016/0166-2236(94)90014-0.

[47] D. Zamanillo, R. Sprengel, Ø. Hvalby, V. Jensen, N. Burnashev, A. Rozov, K.M. M. Kaiser, H.J. Köster, T. Borchardt, P. Worley, J. Lübke, M. Frotscher, P.H. Kelly, B. Sommer, P. Andersen, P.H. Seeburg, B. Sakmann, Importance of AMPA receptors for hippocampal synaptic plasticity but not for spatial learning, Science 284 (1999) 1805–1811, https://doi.org/10.1126/science.284.5421.1805.

[48] H. Adesnik, R.A. Nicoll, Conservation of glutamate receptor 2-containing AMPA receptors during long-term potentiation, J. Neurosci. 27 (2007) 4598–4602, https://doi.org/10.1523/JNEUROSCI.0325-07.2007.

[49] J.T.R. Isaac, M.C. Ashby, C.J. McBain, The role of the GluR2 subunit in AMPA receptor function and synaptic plasticity, Neuron 54 (2007) 859–871, https://doi.org/10.1016/j.neuron.2007.06.001.

[50] H. Sies, Hydrogen peroxide as a central redox signaling molecule in physiological oxidative stress: oxidative eustress, Redox Biol. 11 (2017) 613–619, https://doi.org/10.1016/j.redox.2016.12.035.

[51] M.P. Murphy, H. Bayir, V. Belousov, C.J. Chang, K.J.A. Davies, M.J. Davies, T. P. Dick, T. Finkel, H.J. Forman, Y. Janssen-Heininger, D. Gems, V.E. Kagan, B. Kalyanaraman, N.-G. Larsson, G.L. Milne, T. Nyström, H.E. Poulsen, R. Radi, H. Van Remmen, P.T. Schumacker, P.J. Thornalley, S. Toyokuni, C.C. Winterbourn, H. Yin, B. Halliwell, Guidelines for measuring reactive oxygen species and oxidative damage in cells and in vivo, Nat Metab 4 (2022) 651–662, https://doi.org/10.1038/s42255-022-00591-z.

[52] D. Pattison, M. Davies, Reactions of myeloperoxidase-derived oxidants with biological substrates:gaining chemical insight into human inflammatory diseases, Comput. Mater. Continua (CMC) 13 (2006) 3271–3290, https://doi.org/10.2174/092986706778773095.

[53] B. Halliwell, A. Adhikary, M. Dingfelder, M. Dizdaroglu, Hydroxyl radical is a significant player in oxidative DNA damage *in vivo*, Chem. Soc. Rev. 50 (2021) 8355–8360, https://doi.org/10.1039/D1CS00044F.

[54] R. Radi, Oxygen radicals, nitric oxide, and peroxynitrite: redox pathways in molecular medicine, Proc. Natl. Acad. Sci. U.S.A. 115 (2018) 5839–5848, https://doi.org/10.1073/pnas.1804932115.

[55] A. Ayala, M.F. Muñoz, S. Argüelles, Lipid Peroxidation: Production, Metabolism, and Signaling Mechanisms of Malondialdehyde and 4-Hydroxy-2-Nonenal, Oxidative Medicine and Cellular Longevity, 2014, pp. 1–31, https://doi.org/10.1155/2014/360438, 2014.

[56] R. Arce-Molina, F. Cortés-Molina, P.Y. Sandoval, A. Galaz, K. Alegría, S. Schirmeier, L.F. Barros, A. San Martín, A highly responsive pyruvate sensor reveals pathway-regulatory role of the mitochondrial pyruvate carrier MPC, Elife 9 (2020), e53917, https://doi.org/10.7554/eLife.53917.

[57] J.M. Seckler, S.J. Lewis, Advances in D-amino acids in neurological research, IJMS 21 (2020) 7325, https://doi.org/10.3390/ijms21197325.

[58] X. Ding, N. Ma, M. Nagahama, K. Yamada, R. Semba, Localization of d-serine and serine racemase in neurons and neuroglias in mouse brain, Neurol. Sci. 32 (2011) 263–267, https://doi.org/10.1007/s10072-010-0422-2.

[59] H. Wolosker, S. Blackshaw, S.H. Snyder, Serine racemase: a glial enzyme synthesizing d -serine to regulate glutamate- *N* -methyl- d -aspartate neurotransmission, Proc. Natl. Acad. Sci. U.S.A. 96 (1999) 13409–13414, https://doi.org/10.1073/pnas.96.23.13409.

[60] E. Kartvelishvily, M. Shleper, L. Balan, E. Dumin, H. Wolosker, Neuron-derived D-serine release provides a novel means to activate N-Methyl-D-aspartate receptors, J. Biol. Chem. 281 (2006) 14151–14162, https://doi.org/10.1074/jbc.M512927200.

[61] S. Moreno, R. Nardacci, A. Cimini, M.P. Cerù, Immunocytochemical localization of D-amino acid oxidase in rat brain, J. Neurocytol. 28 (1999) 169–185, https://doi.org/10.1023/A:1007064504007.

[62] K. Hamase, R. Nagayasu, A. Morikawa, R. Konno, K. Zaitsu, Sensitive high-performance liquid chromatographic assay for d-amino-acid oxidase activity in mammalian tissues using a fluorescent non-natural substrate, 5-fluoro-d-tryptophan, J. Chromatogr. A 1106 (2006) 159–164, https://doi.org/10.1016/j.chroma.2005.08.043.

[63] L. Pollegioni, A. Falbo, M.S. Pilone, Specificity and kinetics of Rhodotorula gracillisd-amino acid oxidase, Biochim. Biophys. Acta Protein Struct. Mol. Enzymol. 1120 (1992) 11–16, https://doi.org/10.1016/0167-4838(92)90418-D.

[64] L. Pollegioni, K. Diederichs, G. Molla, S. Umhau, W. Welte, S. Ghisla, M.S. Pilone, Yeast d -amino acid oxidase: structural basis of its catalytic properties, J. Mol. Biol. 324 (2002) 535–546, https://doi.org/10.1016/S0022-2836(02)01062-8.

[65] S.G.N. Grant, T.J. O'Dell, K.A. Karl, P.L. Stein, P. Soriano, E.R. Kandel, Impaired long-term potentiation, spatial learning, and hippocampal development in *fyn* mutant mice, Science 258 (1992) 1903–1910, https://doi.org/10.1126/science.1361685.

[66] Q.-Q. Li, J. Chen, P. Hu, M. Jia, J.-H. Sun, H.-Y. Feng, F.-C. Qiao, Y.-Y. Zang, Y.-Y. Shi, G. Chen, N. Sheng, Y. Xu, J.-J. Yang, Z. Xu, Y.S. Shi, Enhancing GluN2A-type NMDA receptors impairs long-term synaptic plasticity and learning and memory, Mol. Psychiatr. (2022), https://doi.org/10.1038/s41380-022-01579-7.

[67] N. Uetani, Impaired learning with enhanced hippocampal long-term potentiation in PTPdelta-deficient mice, EMBO J. 19 (2000) 2775–2785, https://doi.org/10.1093/emboj/19.12.2775.

[68] G. D'Aniello, A. Tolino, A. D'Aniello, F. Errico, G.H. Fisher, M.M. Di Fiore, The role of d-aspartic acid and N-Methyl-d-Aspartic acid in the regulation of prolactin

release, Endocrinology 141 (2000) 3862–3870, https://doi.org/10.1210/endo.141.10.7706.
[69] Y. Nagata, R. Konno, A. Niwa, Amino acid levels in d-alanine-administered mutant mice lacking d-amino acid oxidase, Metabolism 43 (1994) 1153–1157, https://doi.org/10.1016/0026-0495(94)90059-0.
[70] P. Pernot, J.-P. Mothet, O. Schuvailo, A. Soldatkin, L. Pollegioni, M. Pilone, M.-T. Adeline, R. Cespuglio, S. Marinesco, Characterization of a yeast d -amino acid oxidase microbiosensor for d -serine detection in the central nervous system, Anal. Chem. 80 (2008) 1589–1597, https://doi.org/10.1021/ac702230w.